ACSNANO
www.acsnano.org
ARTICLE

Scalable Preparation of Multifunctional Fire-Retardant Ultralight Graphene Foams

Chuangang Hu,[†,‡,§] Jiangli Xue,[†,§] Liye Dong,[†] Yue Jiang,[†] Xiaopeng Wang,[†] Liangti Qu,[*,†] and Liming Dai[*,‡]

[†]Beijing Key Laboratory of Photoelectronic/Electrophotonic Conversion Materials, Key Laboratory of Cluster Science, Ministry of Education of China, School of Chemistry, Beijing Institute of Technology, Beijing 100081, P. R. China

[‡]Center of Advanced Science and Engineering for Carbon (Case4Carbon), Department of Macromolecular Science and Engineering, Case School of Engineering, Case Western Reserve University, Cleveland, Ohio 44106, United States

Supporting Information

ABSTRACT: **Traditional flame-retardant materials often show poor tolerance to oxidants, strong acidic/alkaline reagents, organic solvents, along with toxicity problems. Herein, highly fire-retardant ultralight graphene foam has been developed, which possesses not only ultralight and compressible characteristics but also efficient flame-retardant properties, outperforming those traditional polymer, metallic oxide, and metal hydroxide based flame retardant materials and their composites. The newly developed unconventional refractory materials are promising for specific applications as demonstrated by the observed high temperature resistant microwave absorption capability.**

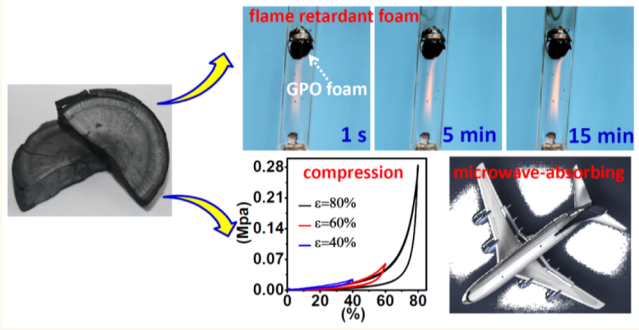

KEYWORDS: *three-dimensional, graphene foam, multifunction, fire resistance*

The development of new materials that can reduce fire risk to save lives and protect property has been attracting a great deal of interest.[1−3] The commonly used organic flame retardant materials often show poor tolerance to oxidants, strong acidic/alkaline regents, and organic solvents, along with toxicity problems.[4,5] Therefore, it is highly desirable to develop flame-retardant materials with good chemical stability and environmentally friendly characteristics. Graphite is the most thermodynamically stable form of the carbon allotropes.[6,7] Superior to graphite in some properties, graphene (a single-layer of graphite) has emerged as a new functional material for construction of various devices because of its excellent electrical conductivity, high surface area, and good chemical, environmental and mechanical stability.[8,9] Graphene-assembled architectures with 3D structure (*e.g.*, foam[8−10]) have a high surface area and can form tunable hierarchical morphology with a lightweight, high porosity, good mechanical stability, and electrical property attractive for a variety of sustainable applications, including energy storage, gas adsorption, and catalysis.[11] Although graphene has been regarded as a flame-retardant additive for polymers with simultaneous improvement of mechanical, thermal, electrical, and gas barrier properties,[12−15] little attention has been paid to systematically investigate flame retardancy of graphene based materials.

In view of the positive role of phosphorus and nitrides in enhancing the flame retardation,[16,17] we herein developed the highly fire-retardant ultralight graphene foam by mixing graphene oxide (GO) solution with hexachlorocyclotriphosphazene (HCTP, molecular formula: $P_3N_3Cl_6$) to form a continuous GO−HCTP (GOTP) foam. Once thermally treated, the resultant graphene−phosphorus oxide/nitride (GPO) foam exhibited not only ultralight and compressible characteristics but also efficient flame-retardant properties, outperforming those traditional polymer, metallic oxide, and metal hydroxide based flame retardant materials and their composites (Table S1). These results are promising for the development of unconventional refractory materials, as demonstrated by the observed high temperature resistant microwave absorption for the newly developed GO−HCTP (GOTP) foam.

RESULTS AND DISCUSSION

Having considerable amounts of hydroxyl, epoxide, carboxyl, and carbonyl functional groups,[18−20] GO sheets disperse well in aqueous solutions and interact strongly with polar components.

Received: October 25, 2015
Accepted: January 8, 2016
Published: January 8, 2016

DOI: 10.1021/acsnano.5b06710
ACS Nano 2016, 10, 1325−1332

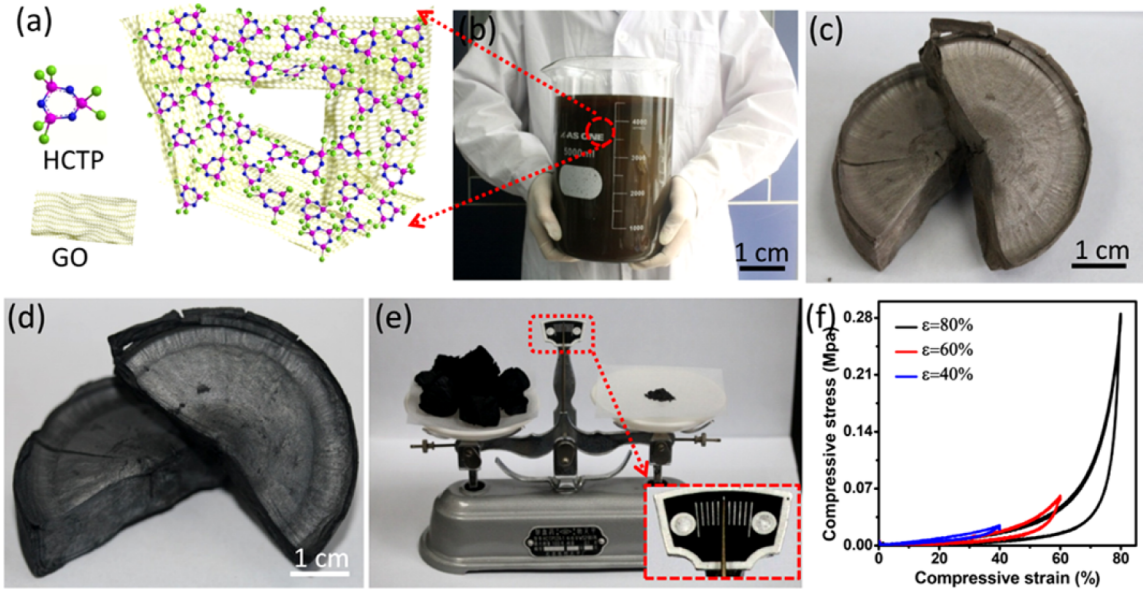

Figure 1. (a) Scheme of HCTP dispersed in GO solution. (b) Photograph of mass GOTP solution. (c, d) The photographs of freeze-dried GOTP foam before and after burning on the flame. (e) GPO foam (left) and graphite power (right) with the same mass on the balance. (f) Stress–strain curves of the GPO foam at different set strains (ε) of 40%, 60%, and 80%, respectively.

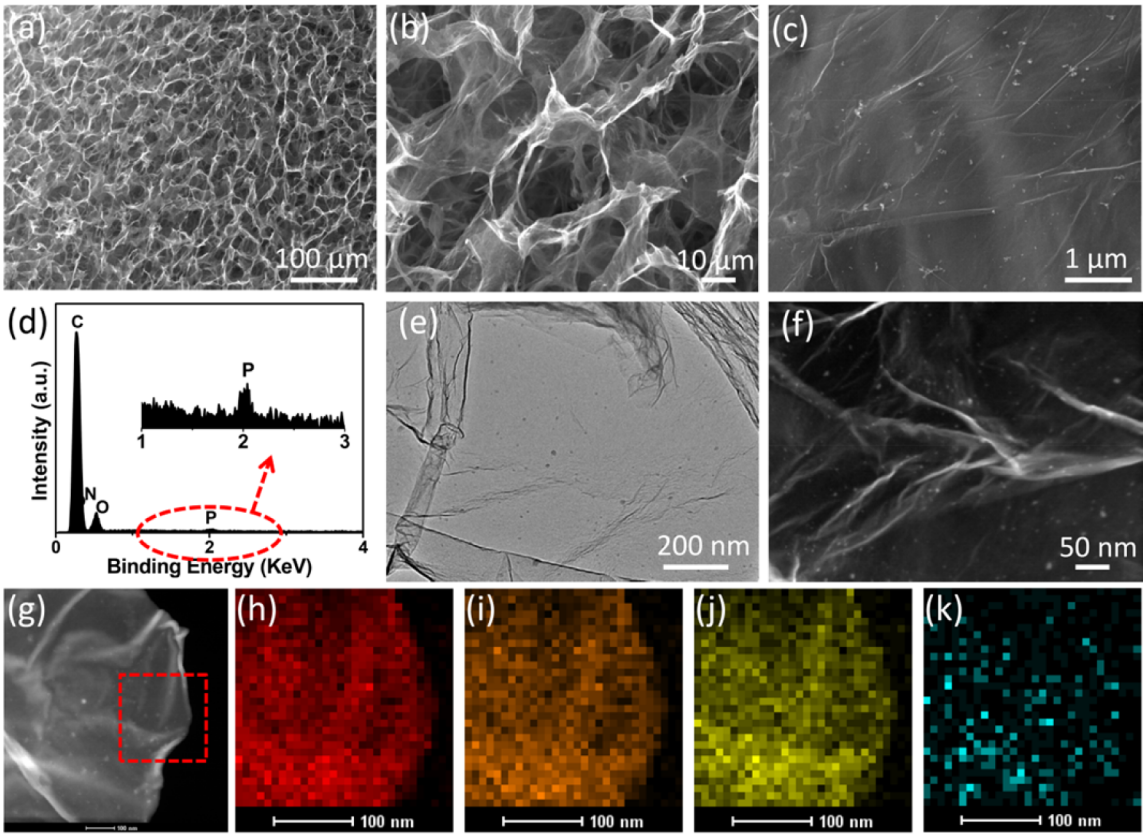

Figure 2. (a–c) SEM images of GPO under different magnifications. (d) Corresponding EDS of the GOTP. (e) TEM image of GPO. (f) Bright-field TEM image of GPO. (g) HAADF-STEM image of a corner of one piece of graphene in GPO. (h–k) HAADF-STEM-EDS mapping images of C, N, O, and P elements, respectively.

As such, the mixture of GO solution and HTCP can form the GOTP foam in mass scale by freeze-drying (Figure 1a–c, Figure S1). Upon thermal treatment (on the outer flame with a temperature of *ca.* 500 °C for 2 min), the C–O/C=O bonds on the GO react with the adsorbed HCTP to form the GPO foam immediately (Figure 1d). Herein, the mass ratio between GO and HCCP was fixed at 10:1. The formed ultralight GOTP foam (density: 2 mg cm^{-3}) with a dark brown color (Figure 1c) exhibits a 3D porous structure of GO sheets (Figures S1a and S2). The homogeneous distribution of P element in the GOTP

DOI: 10.1021/acsnano.5b06710
ACS Nano 2016, 10, 1325–1332

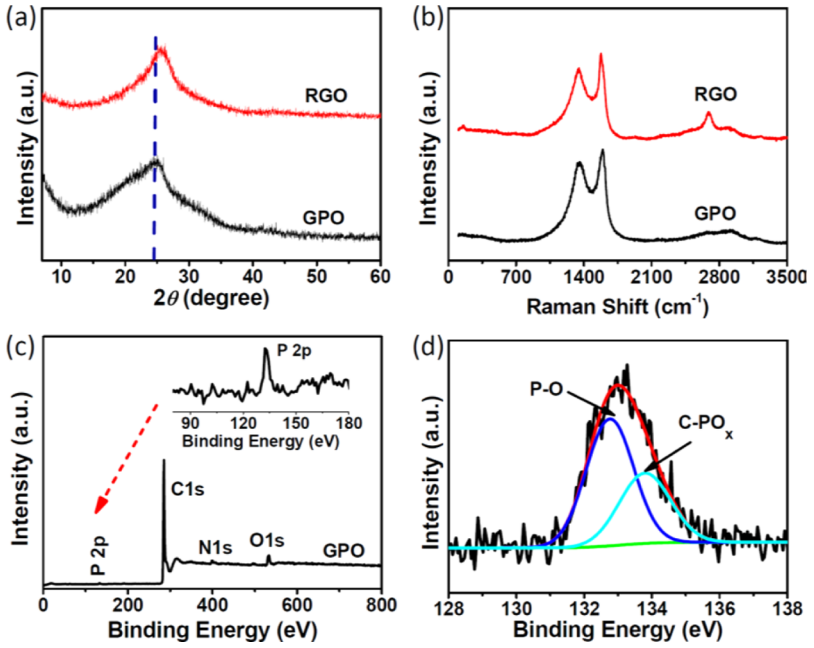

Figure 3. (a) XRD patterns of RGO and GPO. (b) Corresponding Raman spectra. (c) XPS survey of GPO. (d) High-resolution spectrum of P 2p XPS peak in (c).

sample recorded by an enlarged scanning electron microscopic (SEM) imaging (Figure S1b) and the corresponding energy dispersive spectroscopy (EDS) mapping (Figure S1c) indicates that the HCTP organic compound is uniformly anchored on the sheets of 3D GO, and the atomic ratio of C/N/O/P in the GOTP from XPS and EDS analysis is *ca.* 2.1/0.11/1/0.13 (Figure S1d and Figure S3). X-ray diffraction (XRD) patterns of GO and GOTP also indicate that HCTP has been homogeneously intercalated into GO interlayers without phase separation (Figure S1e,f). GOTP foam was converted into the GPO instantly by a simple treatment with a hot flame (Figure 1c,d). The resultant GPO foam has an ultralight 3D framework with a density of *ca.* 1 mg cm^{-3}. A four-probe electrical resistance of *ca.* 9000 Ω is obtained for the GPO foam, and the moderate resistance is most likely due to its loose 3D structure. Additionally, the GPO foam exhibits a thermal conductivity of 20 mW m^{-1} K^{-1},[21] which is a relatively small value among the flame-retardant materials, which is beneficial to prevent thermal diffusion and, thus, enhance its retardant properties.

As shown in Figure 1f, the GPO foam with the same mass as that of the graphite powder at the opposite end of a pair of scales shows a much larger volume than that of the graphite powder, indicating a potentially high compressibility for the GPO. Indeed, GPO foam can sustain large-strain deformations (*e.g.*, ε = 40%) under manual compression and recover most of the original volume without structural fatigue (Figure 1f). Compression tests at differently set strains (40−80%) show reproducible results in which all stress−strain curves contain an approximate linear region at initial ε < 40%, which can be explained by the high strength and modulus of graphene sheets of the macropores;[22,23] the large strain should induce heavy bending and buckling of graphene pore walls; and the loading curve is flatten as expected. The successive short linear region with a steeper slope between 40% and 53% is caused by the high membrane stresses of graphene sheets. Although the tensile strength of graphene is high, its elongation at the break is smaller than that of an elastic polymer. Therefore, this region was short and followed an inflection point of 53%, indicating the graphene sheets were torn and partially irreversibly damaged.[23] The unloading curves almost return to the origin, indicating a complete volume recovery without any plastic deformation. The observed high compressibility of the GPO foam is attributable to inherent pore-rich structures, rather than the possible formation of densely stacked graphene sheets *via* strong $\pi-\pi$ interaction under compression as in the case of the pure 3D graphene with an irreversible compressibility.[24] Therefore, the highly uniform deposition of HCTP layers among GO sheets has facilitated the formation of the well-defined 3D porous structures and ensures the structural strength to achieve the compression-tolerant foam feature.

As shown in Figure 2, the field-emission SEM (FE-SEM) images (Figures 2a−c) indicate that the thermally reduced GO maintain an incompact but highly cross-linking 3D porous structure as that of the GOTP without any collapse. The EDS in Figure 2d reveals the presence of C, O, and P elements with an atomic ratio of C/N/O/P in the GOTP sample to be *ca.* 13.1/0.59/1/0.27, indicating an effective reduction of GO. The inset in Figure 2d further confirms the existence of a small amount of P element. The morphology of GPO was confirmed by transmission electron microscopy (TEM) images in Figure 2e,f and high-resolution TEM (HR-TEM) in Figure S4, in which nanoparticles with a size of less than 5 nm were revealed to homogeneously anchor onto the graphene sheets. This is also confirmed by the bright-field TEM image (Figure 2f) of a piece of graphene sheet. Since small nanoparticles are composed of heavier elements (P, N) than surrounding graphene (C), they appear darker in the bright-field TEM image.[15] The high-angle annular bright-field scanning transmission electron microscopy (HAABF-STEM, Figure 2g) and the corresponding elemental mappings (Figure 2h−k) further reveal that C, N, and O elements are coexistent and evenly distributed over the graphene sheet, along with P-containing nanoparticles on the graphene surface.

DOI: 10.1021/acsnano.5b06710
ACS Nano 2016, 10, 1325−1332

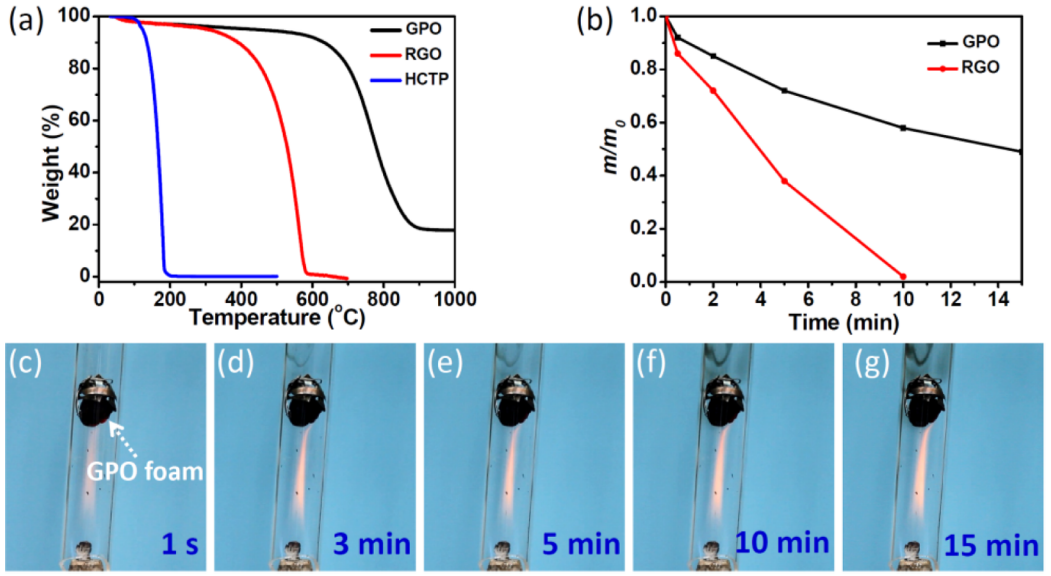

Figure 4. (a) TGA curves of GPO, RGO, and HCTP were conducted under air atmosphere. (b) Mass loss as a function of the burning time for GPO and RGO on the flame of alcohol lamp. (c–g) Photographs of the GPO foam flowing on the out flame with different times (the GPO was confined in a quartz tube).

XRD patterns of RGO and GPO confirm the representative peak of GO ($2\theta \approx$ *ca.* 11°, Figure S1e)[25,26] has completely disappeared in the as-obtained GPO, accompanied by a new broad peak centered at *ca.* 24.8° (the bottom curve in Figure 3a), corresponding to the (002) plane of stacked graphene sheets with an interlayer spacing of 0.358 nm. This value is larger than the displacement (0.346 nm) of RGO ($2\theta \approx$ *ca.* 25.7°, the upper curve in Figure 3a), suggesting the uncompact stacking of graphene sheets in the GPO with P-containing nanoparticles. Raman spectra of GPO and RGO (Figure 3b) show the clearly separated G-band at 1596 cm^{-1} and D-band located at 1347 cm^{-1}, with an I_D/I_G ratio of 0.90 for GPO and 0.81 for RGO plus a sharp 2D-band peak at 2692 cm^{-1} for RGO only. These results clearly indicate that there might be a interaction between the graphene structure and the P-containing nanoparticles.[27] XPS survey of GPO (Figure 3c) and amplified region of P (inset in Figure 3c) indicate, once again, the sample is mainly composed of C, O, N, and P elements. The atomic ratio of C/N/O/P in the sample calculated from the XPS survey spectrum is *ca.* 12.5/0.61/1/0.23, matched well with the EDS data. Furthermore, the high-resolution (HR) P 2p XPS spectra of GOPT and GPO (Figure 3d and Figure S5) were collected to gain more insight into phosphorus doping. It reveals that the predominant P–Cl bond (133.9 eV) in HCTP has been replaced and the coexistence of both C-PO_x (133.8 eV) and P–O (132.8 eV) bonds in the GPO, which has been widely regarded as the critical factor for flame retardant.[28,29] Because of the relatively large atomic radius of Cl and the large difference in chemical properties between C and Cl, the insertion of Cl in the graphene skeleton seems impossible during a short thermal treatment, and hence, the Cl element was not found in the final GPO foam (Figure S6). However, the doping of N element in the graphene was demonstrated by the HR-XPS spectrum of N 1s (Figure S7).

Figure 4a shows the thermogravimetric analysis (TGA) curves of RGO, GPO, and HCTP measured in air with a heating rate of 10 °C min^{-1}. As can be seen, the GPO composite shows a higher decomposition temperature compared with those of RGO and HCTP. The GPO shows a T_{10} (the temperature of 10% decomposition) of 662 °C, which is higher than that of RGO (426 °C) by *ca.* 236 °C. At 700 °C, the instant amount of residue is 82% for GPO whereas only 1% for RGO, suggesting a much slower oxidative degradation of GPO. This value of 82% for GPO is also much higher than that of polymer, metallic oxide, metal hydroxide based flame-retardant materials and their composites, as summarized in Table S1.[15,21,30–34] The residual weight percentage of GPO at a temperature of up to 1000 °C in air is still 18%, while RGO and HCTP samples are fully oxidized or decomposed before 700 and 200 °C, respectively. The thermal stability of GPO and RGO was also assessed on a hot flame (Figure 4b) up to 15 min, which caused only a slight mass loss from GPO, whereas RGO lost 100% of its initial mass in just 10 min. The GOTP foam synthesized in this study has a 3D interconnected porous structure (*vide supra*), which effectively maximizes the accessibility of HCTP to the graphene surface to prevent the structural collapse of graphene sheets from serious oxygen etching (Figures S8 and S9), making GPO (even with an extremely limited amount of HCTP) far more stable than RGO. Therefore, the observed enhancement in fire-retardance for the GPO foam can be attributed to its unique 3D structure. Figure 4c–g displays the photographs of the GPO foam flown on the flame with different times. To prevent the GPO foam from flying out the quartz tube during burning, a Cu mesh was placed above the GPO foam in a suitable position along the quartz tube. The photographs taken for the first 3 min (Figure S10) and the enlarged views of the GPO foam for long time flame retardant test (15 min, Figure 4e–g) further show that the GPO foam on the flame did not change in appearance, demonstrating a high thermal stability of the GPO foam. A simple comparison of the photograhs for the GPO and RGO foams directly on the flam for different times (Figure S11) also indicated that the compound GPO has excellent flame-retardant properties.

It was found that the incorporation content of P in the GPO was not changed with the increased amount of raw material (HCCP), as the additional HCCP decomposed completely. For example, for samples with different mass ratios between GO

DOI: 10.1021/acsnano.5b06710
ACS Nano 2016, 10, 1325–1332

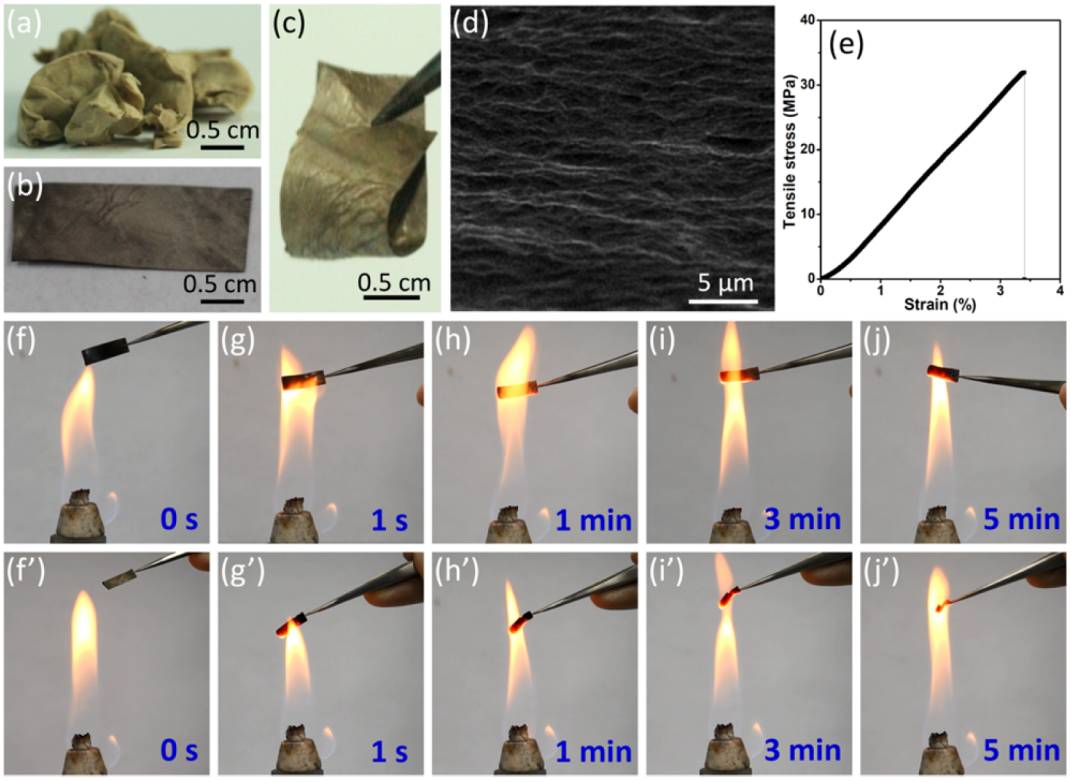

Figure 5. (a) Photographs of deliberately cracked GOTP carvings. (b, c) GOTP film. (d) SEM image of the GOTP film. (e) Typical stress–strain curve of the as-prepared GOTP film. (f–j) Photographs of a GOTP film on a hot flame with different times. (f′–j′) Pure GO film on a hot flame with different times.

and HCCP (*e.g.*, 10:1, 5:1, 2.5:1) on the outer flame with a temperature of *ca.* 500 °C for 20 s, the density of the N,P-containing particles varies (Figure S12). However, when the reaction was prolonged to 2 min, all of the obtained samples had a similar composition. Even at a high mass ratio of 2.5:1, the content of P in the obtained GPO was just 1.9% (Figure S13). Of course, when the content of raw material (HCCP) in the GOTP was extremely low, *e.g.*, 4.7 wt %, the P content in GPO was almost negligible (Figure S14). The mechanical strength and the TGA analysis of the samples of GO/HCTP with different mass ratios are presented in Figures S15 and S16, respectively. It was found that HCTP in the GOTP will result in some changes of the 3D structures (Figure S17) and, thus, worse performance in mechanical strength and flame retardant property. Therefore, the HCCP in GOTP was fixed at *ca.* 9 wt %.

The ultralight foam structure of GOTP (Figure 5a–c) can be converted into flexible thin films (Figure 5b) by simply pressing the 3D GOPT with relatively large pressure (*e.g.*, 40 MPa), resulting in the formation of fire-retardant films. The SEM image in Figure 5d reveals that the zigzag buckles without cracks were formed along the GOTP film, making the film tolerate a certain extra force as shown in Figure 5e (*cf.* Figure 1f). The GOTP film has a tensile strength of up to 32 MPa with a typical elongation at break of *ca.* 3.4%, presumably originating from the possible displacement of the graphene sheets within the film.[35] Parts f–j of Figure 5 display the photographs for a GOTP film on a hot flame for different times. The shape of the GOPT film (Figure S18) maintained well even after burning on the outer flame of the alcohol lamp for 5 min. On the contrary, pure GO film became unstable on the flame and was burned out at 5 min (Figure 5f′–j′).

Microwave-absorbing materials are currently in high demand for many expanded electromagnetic interference shielding and radar cross section reduction applications for both commercial and defense purposes. However, conventional microwave-absorbing materials are usually heavy and bulky, which limits their applications, especially in aircrafts. Here, the lightweight, flame-retardant GPO materials provide a promising candidate for the development of new types of microwave-absorbing materials and devices. Those features GOP materials owned make them are highly tolerant toward high temperature and suitable for the application in the aerospace industry. Microwave absorption is mainly attributed to two types of contributions: dielectric loss and magnetic loss.[36] To investigate the performance of microwave absorption of the GPO flame-retardant material, we measured both the complex relative permittivity (ε) and permeability (μ) of the sample associated with the dielectric loss and magnetic loss, respectively.[37,38] Figures S19 and S20 show the real and imaginary parts of the complex relative permittivity (ε', ε'') and permeability (μ', μ'') measured for the samples before and after burning on a hot flame for frequencies between 26.5 and 40.0 GHz. The simulated microwave reflection loss (RL) *versus* frequency was obtained according to the transmission line theory by eqs 1 and 2 in the Methods section. Accordingly, the RL of GPO before and after burning is shown in Figure S21. The samples of GPO before and after burning show similar wave-absorbing abilities, and the dielectric constant of GPO gradually decreased as the frequency increased within the range of 26.5–40.0 GHz from the complex permittivity and permeability. The absorption peaks for the samples of GPO before and after burning are less than −6.4 and −8.4 dB. Obviously, there were two strong wave-absorbing peaks at 37.8 and 38.5 GHz, and the minimum

DOI: 10.1021/acsnano.5b06710
ACS Nano 2016, 10, 1325–1332

reflection loss of GPO before and after burning reached about 30.6−37.2 and 35.7−42.4 eV, respectively, indicating an excellent microwave absorption capacity. The GPO with a large contact surface and 3D structure acts as an excellent substrate for the effective absorption of microwaves. Furthermore, the enhanced both dielectric loss and magnetic loss of GPO after burning caused slightly better electromagnetic wave absorption characteristics.

CONCLUSIONS

In summary, GOTP foams (HCTP functionalized GO) has been successfully synthesized *via* a facile freeze-drying-assisted strategy, which has advantages in terms of manufacturing simplicity, scalability, and environment friendliness. Upon exposure to flame, the resultant HCTP-functionalized GO spontaneously converted into 3D graphene decorated with P- and N-containing nanoparticles. The resulting GPO exhibited an efficient flame-retardant feature, plus an ultralight, compressible structure and microwave absorption capacity, which make them useful for various applications particularly as potential candidates in the aerospace industry.

METHODS

Synthesis of GO. GO was prepared from natural graphite powder *via* acid-oxidation according to a modified Hummers method.[39−41]

Synthesis of GO−GOTP Foam. GO solution was mixed well with HCTP; after freeze-drying, HCTP adsorbed on the surface of GO sheets *in situ*, producing the continuous foam of GOTP. The mass ratio between GO and HCCP for a typical experiment was fixed at 10:1. For comparison, GOTP samples with different mass ratios between GO and HCCP (eg., 20:1, 5:1, 2.5:1) were prepared.

Synthesis of GPO/Nitrides and RGO. After the heat-treatment process (on the outer flame of alcohol lamp with a temperature of *ca.* 500 °C for 2 min), GOTP foams were quickly converted into GPO foams.

For comparison, RGO foams were obtained in the absence of HCTP under experimental conditions identical to those used in the preparation of GPO.

The samples were characterized by X-ray diffraction (XRD) on a D/max-2200/PC X-ray diffractometer with a Cu K radiation source. The particle size and morphology of the samples were determined by JEOL-100CX high-resolution transmission electron microscopy (HR-TEM) at an acceleration voltage of 200 kV. Thermogravimetric analysis (TGA) was performed on a NETZSCH STA 449C. Raman spectroscopy (Renishaw Rm-1000) was conducted with a He/Ne laser at a wavelength of 457.5 nm. Microwave scattering parameters (S parameter, S_{ij}, i, j = 1, 2) were measured using an Agilent E8363B vector network analyzer (VNA) in the frequency range of 2−18 GHz. Complex permittivity ($\varepsilon_r = \varepsilon' - j\varepsilon''$) was calculated from the S parameters according to the literature.[42,43] The tests of magnetic properties were carried out using Lake Shore's vibrating sample magnetometer (VSM model 7307).

Microwave Absorption Test. To investigate the performance of microwave absorption of the flame retardant material, we independently measured the complex relative permittivity (ε) and permeability (μ) of the sample. The reflection loss curves for these samples were calculated with two formulas[36,40]

$$RL(\mathrm{dB}) = 20 \log \left| \frac{z_{in} - 1}{z_{in} + 1} \right| \quad (1)$$

where z_{in} is the normalized input impedance calculated with the following formula

$$z_{in} = \sqrt{\mu_r/\varepsilon_r}\, \tan h[j(2\pi/c)\sqrt{\mu_r \varepsilon_r}\, d] \quad (2)$$

where c is the speed of light, d is the thickness of sample, and f is the microwave frequency. Apparently, reflection loss is significantly influenced by complex relative permittivity and μ_r permeability ε_r of test sample. It should be noted that direct data collected from the test facility (vector network analyzer) is the real part of permittivity μ', the imaginary μ'' and the real part of permeability ε', and the imaginary part of permeability ε''. As important parameters for microwave absorption properties, the real part (ε') and imaginary part (ε'') of complex permittivity of the samples were measured in the frequency range of 26.5−40 GHz in this work. To obtain the complex relative permittivity and permeability, two additional equations are used:[43]

$$\mu_r = \mu' - j\mu'' \quad (3)$$

and

$$\varepsilon_r = \varepsilon' - j\varepsilon'' \quad (4)$$

After solving these two equations we obtained the values of μ_r and ε_r. To examine the microwave absorption properties of these samples, a certain amount of the test sample was mixed with paraffin wax, after thorough stirring at 90°, a mold was used and the mixture was made into a test model following a typical measurement procedure in order to combine powder- or paper-like materials together.

ASSOCIATED CONTENT

Supporting Information

The Supporting Information is available free of charge on the ACS Publications website at DOI: 10.1021/acsnano.5b06710.

Characterization of GOTP including SEM images, EDS mapping, XRD patterns and XPS survey; photograph and SEM images of GO foam; HR-TEM image of GPO; HR-XPS spectra of P, Cl, and N elements in GOTP or GPO; TEM and SEM images of RGO after burning treatment; photographs of the GPO foam flow on the out flame with different times; photographs of GOTP and GO foams on a hot flame with different times; photograph of GOTP film after burning; frequency dependence of the real and imaginary parts of complex permittivity/permeability for GPO foam before and after burning *vs* frequency; comparison of the microwave absorption performance for GPO before and after burning on the flame (PDF)

AUTHOR INFORMATION

Corresponding Authors

*E-mail: lqu@bit.edu.cn.

*E-mail: liming.dai@case.edu.

Author Contributions

§These authors contributed equally to this work.

Notes

The authors declare no competing financial interest.

ACKNOWLEDGMENTS

This work was supported by NSFC (Nos. 21325415 and 21174019), the National Basic Research Program of China (2011CB013000), and the Beijing Natural Science Foundation (2152028).

REFERENCES

(1) Chen, S. S.; Li, X.; Li, Y.; Sun, J. Q. Intumescent Flame-Retardant and Self-Healing Superhydrophobic Coatings on Cotton Fabric. *ACS Nano* **2015**, *9*, 4070−4076.

(2) Weil, E. D.; Levchik, S. V. *Flame Retardants for Plastics and Textiles: Practical Applications*; Carl Hanser Verlag: Cincinnati, 2009.

(3) Lu, S. Y.; Hamerton, I. Recent Developments in the Chemistry of Halogen-Free Flame Retardant Polymers. *Prog. Polym. Sci.* **2002**, *27*, 1661−1712.

DOI: 10.1021/acsnano.5b06710
ACS Nano 2016, 10, 1325−1332

(4) Kandola, B. K.; Krishnan, L.; Deli, D.; Ebdon, J. R. Blends of Unsaturated Polyester and Phenolic Resins for Application as Fire-Resistant Matrices in Fibre-Reinforced Composites. Part 2: Effects of Resin Structure, Compatibility and Composition on Fire Performance. *Polym. Degrad. Stab.* **2015**, *113*, 154−167.
(5) Attia, N. F.; Hassan, M. A.; Nour, M. A.; Geckeler, K. E. Flame-Retardant Materials: Synergistic Effect of Halloysite Nanotubes on the Flammability Properties of Acrylonitrile−Butadiene−Styrene Composites. *Polym. Int.* **2014**, *63*, 1168−1173.
(6) Kennedy, C. S.; Kennedy, G. C. The Equilibrium Boundary between Graphite and Diamond. *J. Geophys. Res.* **1976**, *81*, 2467−2470.
(7) Knox, B. E.; Palmer, H. B. Bond Dissociation Energies in Small Hydrocarbon Molecules. *Chem. Rev.* **1961**, *61*, 247−255.
(8) Chen, W.; Li, S.; Chen, C.; Yan, L. Self-Assembly and Embedding of Nanoparticles by *in Situ* Reduced Graphene for Preparation of a 3D Graphene/Nanoparticle Aerogel. *Adv. Mater.* **2011**, *23*, 5679−5683.
(9) Chen, Z. P.; Ren, W. C.; Gao, L. B.; Liu, B. L.; Pei, S. F.; Cheng, H. M. Three-Dimensional Flexible and Conductive Interconnected Graphene Networks Grown by Chemical Vapour Deposition. *Nat. Mater.* **2011**, *10*, 424−428.
(10) Hu, C. G.; Cheng, H. H.; Zhao, Y.; Hu, Y.; Liu, Y.; Dai, L. M.; Qu, L. T. Newly-Designed Complex Ternary Pt/PdCu Nanoboxes Anchored on Three-Dimensional Graphene Framework for Highly Efficient Ethanol Oxidation. *Adv. Mater.* **2012**, *24*, 5493−5498.
(11) Hu, C. G.; Zheng, G. P.; Zhao, F.; Shao, H. B.; Zhang, Z. P.; Chen, N.; Jiang, L.; Qu, L. T. A Powerful Approach to Functional Graphene Hybrids for High Performance Energy-Related Application. *Energy Environ. Sci.* **2014**, *7*, 3699−3708.
(12) Wang, J. Q.; Han, Z. D. The Combustion Behavior of Polyacrylate Ester/Graphite Oxide Composites. *Polym. Adv. Technol.* **2006**, *17*, 335−340.
(13) Uhl, F. M.; Yao, Q.; Nakajima, H.; Manias, E.; Wilkie, C. A. Expandable Graphite/Polyamide-6 Nanocomposites. *Polym. Degrad. Stab.* **2005**, *89*, 70−84.
(14) Li, Z. Z.; Qu, B. J. Flammability Characterization and Synergistic Effects of Expandable Graphite with Magnesium Hydroxide in Halogen-Free Flame-Retardant EVA Blends. *Polym. Degrad. Stab.* **2003**, *81*, 401−408.
(15) Fang, B.; Peng, L.; Xu, Z.; Gao, C. Wet-Spinning of Continuous Montmorilonite-Graphene Fibers for Fire-Resistant Lightweight Conductors. *ACS Nano* **2015**, *9*, 5214−5222.
(16) Wen, P. Y.; Wang, X. F.; Wang, B. B.; Yuan, B. H.; Zhou, K. Q.; Song, L.; Hu, Y. A.; Yuen, R. K. K. One-Pot Synthesis of a Novel s-Triazine-Based Hyperbranched Charring Foaming Agent and Its Enhancement on Flame Retardancy and Water Resistance of Polypropylene. *Polym. Degrad. Stab.* **2014**, *110*, 165−174.
(17) Nguyen, T. M. D.; Chang, S.; Condon, B.; Uchimiya, M.; Graves, E.; Smith, J.; Easson, M.; Wakelyn, P. Synthesis and Characterization of a Novel Phosphorus-Nitrogen-Containing Flame Retardant and Its Application for Textile. *Polym. Adv. Technol.* **2012**, *23*, 1036−1044.
(18) Li, C.; Shi, G. Q. Functional Gels Based on Chemically Modified Graphenes. *Adv. Mater.* **2014**, *26*, 3992−4012.
(19) Chen, D.; Feng, H.; Li, J. Graphene Oxide: Preparation, Functionalization, and Electrochemical Applications. *Chem. Rev.* **2012**, *112*, 6027−6053.
(20) Edwards, R. S.; Coleman, K. S. Graphene Synthesis: Relationship to Applications. *Nanoscale* **2013**, *5*, 38−51.
(21) Wicklein, B.; Kocjan, A.; Salazar-Alvarez, G.; Carosio, F.; Camino, G.; Antonietti, M.; Bergström, L. Thermally Insulating and Fire-Retardant Lightweight Anisotropic Foams Based on Nanocellulose and Graphene oxide. *Nat. Nanotechnol.* **2015**, *10*, 277−283.
(22) Li, Y. R.; Chen, J.; Huang, L.; Li, C.; Hong, J. D.; Shi, G. Q. Highly Compressible Macroporous Graphene Monoliths *via* an Improved Hydrothermal Process. *Adv. Mater.* **2014**, *26*, 4789−4793.
(23) Xu, Y. X.; Sheng, K. X.; Li, C.; Shi, G. Q. Self-Assembled Graphene Hydrogel *via* a One-Step Hydrothermal Process. *ACS Nano* **2010**, *4*, 4324−4330.
(24) Zhao, Y.; Liu, J.; Hu, Y.; Cheng, H. H.; Hu, C. G.; Jiang, C. C.; Jiang, L.; Cao, A. Y.; Qu, L. T. Highly Compression-Tolerant Supercapacitor Based on Polypyrrole-Mediated Graphene Foam Electrodes. *Adv. Mater.* **2013**, *25*, 591−595.
(25) Pavlidou, S.; Papaspyrides, C. D. A Review on Polymer−Layered Silicate Nanocomposites. *Prog. Polym. Sci.* **2008**, *33*, 1119−1198.
(26) Hu, C. G.; Zhai, X. Q.; Liu, L.; Zhao, Y.; Jiang, L.; Qu, L. T. Spontaneous Reduction and Assembly of Graphene Oxide into Three-Dimensional Graphene Network on Arbitrary Conductive Substrates. *Sci. Rep.* **2013**, *3*, 2065.
(27) Hu, C. G.; Xiao, Y.; Zhao, Y.; Chen, N.; Zhang, Z. P.; Cao, M. H.; Qu, L. T. Highly Nitrogen-Doped Carbon Capsules: Scalable Preparation and High-Performance Applications in Fuel Cells and Lithium Ion Batteries. *Nanoscale* **2013**, *5*, 2726−2733.
(28) Kim, M. J.; Jeon, I. Y.; Seo, J. M.; Dai, L. M.; Baek, J. B. Graphene Phosphonic Acid as an Efficient Flame Retardant. *ACS Nano* **2014**, *8*, 2820−2825.
(29) Ma, X.; Ning, G.; Qi, C.; Xu, C.; Gao, J. Phosphorus and Nitrogen Dual-Doped Few-Layered Porous Graphene: A High-Performance Anode Material for Lithium-Ion Batteries. *ACS Appl. Mater. Interfaces* **2014**, *6*, 14415−14422.
(30) Hu, W. Z.; Yu, B.; Jiang, S. D.; Song, L.; Hu, Y.; Wang, B. B. Hyper-Branched Polymer Grafting Graphene Oxide as an Effective Flame Retardant and Smoke Suppressant for Polystyrene. *J. Hazard. Mater.* **2015**, *300*, 58−66.
(31) Yang, H. F.; Gong, J.; Wen, X.; Xue, J.; Chen, Q.; Jiang, Z. W.; Tian, N. N.; Tang, T. Effect of Carbon Black on Improving Thermal Stability, Flame Retardancy and Electrical Conductivity of Polypropylene/Carbon Fiber Composites. *Compos. Sci. Technol.* **2015**, *113*, 31−37.
(32) Beheshti, A.; Heris, S. Z. Experimental Investigation and Characterization of an Efficient Nanopowder-Based Flame Retardant Coating for Atmospheric-Metallic Substrates. *Powder Technol.* **2015**, *269*, 22−29.
(33) Costes, L.; Laoutid, F.; Dumazert, L.; Lopez-cuesta, J.; Brohez, S.; Delvosalle, C.; Dubois, P. Metallic Phytates as Efficient Bio-Based Phosphorous Flame Retardant Additives for Poly (Lactic Acid). *Polym. Degrad. Stab.* **2015**, *119*, 217−227.
(34) Chen, X. E.; Liu, L.; Jiao, C. M. Influence of Iron Oxide Brown on Smoke-Suppression Properties and Combustion Behavior of Intumescent Flame-Retardant Epoxy Composites. *Adv. Polym. Technol.* **2015**, DOI: 10.1002/adv.21516.
(35) Hu, C. G.; Zhao, Y.; Cheng, H. H.; Wang, Y. H.; Dong, Z. L.; Jiang, C. C.; Zhai, X. Q.; Jiang, L.; Qu, L. T. Graphene Microtubings: Controlled Fabrication and Site-Specific Functionalization. *Nano Lett.* **2012**, *12*, 5879−5884.
(36) Hu, C. G.; Mou, Z. Y.; Lu, G. W.; Chen, N.; Dong, Z. L.; Hu, M. J.; Qu, L. T. 3D graphene−Fe_3O_4 Nanocomposites with High-Performance Microwave Absorption. *Phys. Chem. Chem. Phys.* **2013**, *15*, 13038−13043.
(37) Kim, S. S.; Jo, S. B.; Choi, K. K.; Kim, J. M.; Churn, K. S. Complex Permeability and Permittivity and Microwave Absorption of Ferrite-rubber Composite at X-Band Frequencies. *IEEE Trans. Magn.* **1991**, *27*, 5462−5464.
(38) Liu, J. R.; Itoh, M.; Machida, K. I. Electromagnetic Wave Absorption Properties of α-Fe/Fe_3B/Y_2O_3 Nanocomposites in Gigahertz Range. *Appl. Phys. Lett.* **2003**, *83*, 4017−4019.
(39) Hummers, W.; Offeman, R. Preparation of Graphitic Oxide. *J. Am. Chem. Soc.* **1958**, *80*, 1339−1339.
(40) Kovtyukhova, N.; Ollivier, P.; Martin, B.; Mallouk, T.; Chizhik, S.; Buzaneva, E.; Gorchinskiy, A. Layer-by-Layer Assembly of Ultrathin Composite Films From Micron-Sized Graphite Oxide Sheets and Polycations. *Chem. Mater.* **1999**, *11*, 771−778.
(41) Cote, L.; Kim, F.; Huang, J. Langmuir−Blodgett Assembly of Graphite Oxide Single Layers. *J. Am. Chem. Soc.* **2009**, *131*, 1043−1049.

DOI: 10.1021/acsnano.5b06710
ACS Nano 2016, 10, 1325−1332

(42) Kwon, H. J.; Shin, J. Y.; Oh, J. H. The Microwave Absorbing and Resonance Phenomena of Y-Type Hexagonal Ferrite Microwave Absorbers. *J. Appl. Phys.* **1994**, *75*, 6109−6111.
(43) Nicolson, A. M.; Ross, G. F. Measurement of the Intrinsic Properties of Materials by Time-Domain Techniques. *IEEE Trans. Instrum. Meas.* **1970**, *19*, 377−382.

DOI: 10.1021/acsnano.5b06710
ACS Nano 2016, 10, 1325−1332